International Journal of Computational Intelligence Systems
Vol. **14(1)**, 2021, *pp.* 1208–1216
DOI: https://doi.org/10.2991/ijcis.d.210318.002; ISSN: 1875-6891; eISSN: 1875-6883
https://www.atlantis-press.com/journals/ijcis/

Research Article

The Mathematical Model and Deep Learning Features Selection for Whorl Fingerprint Classifications

Ibrahim Jawarneh[1], Nesreen Alsharman[2,*]

[1]*Department of Mathematics, Al-Hussein Bin Talal University, Ma'an, Jordan*
[2]*Computer Science, The World Islamic Sciences and Education University, Amman, Jordan*

ARTICLE INFO

Article History
Received 08 Jan 2021
Accepted 14 Mar 2021

Keywords
Whorl fingerprint
Classes of whorl fingerprint
Simulations of dynamical system for whorl fingerprint
Convolutional neural networks architectures

ABSTRACT

In this paper, different classes of the whorl fingerprint are discussed. A general dynamical system with a parameter θ is created using differential equations to simulate these classes by varying the value of θ. The global dynamics is studied, and the existence and stability of equilibria are analyzed. The Maple is used to visualize fingerprint's orientation image as a smooth deformation of the phase portrait of a planar dynamical system. In general, the databases of fingerprint are not categorized to retained by artificial intelligence tools such Convolutional Neural Networks (CNNs) architectures, so finding a dynamical system to categorize fingerprint database of fingerprints images allows CNNs architectures to retrained with more accuracy. NIST Special Database (SD) 302d fingerprint dataset is retrained over VGG16 as CNN architecture.

1. INTRODUCTION

Fingerprints are a set of raised lines that form unique patterns on the pads of the fingers and thumbs. Everyone leaves parts or entire fingerprints on many things through our daily activities by touching cups, doors, books, etc., so studying fingerprints is important in security especially no two people have been found to have the same fingerprints. One of the early studies about fingerprints appeared in 1892 by Sir Francis Galton in his book, finger prints [1]. There are three general types of fingerprints; loop, whorl, and arch. The whorl type occurs in about 25–35% of all fingerprints, see [1–3].

The whorl patterns display in the way that the ridges in the center tend to show a circular orientation with a core to whorl and two deltas in the right and left sides. The focus of this paper is on three basic categories of whorl fingerprint which are concentric whorl, spiral whorl, and composite whorl with "S" core:

- Concentric whorl, this pattern represents the most basic form of a whorl in which the core is circular or elliptical in the center of the fingerprint, see picture (a) in Figure 1.
- Spiral whorl, the ridges flow are in winding way in the center making a spiral core, see picture (b) and (c) in Figure 1.
- Composite whorl with "S" core, this pattern twists its ridges in the way that forms a core in "S" shape in the center, see picture (d) in Figure 1.

Many fingerprint classification algorithms were developed [7–16]. Among these, the usual features used are singularities and orientation image information, the combining of these features is common. In Dass and Jain [17], a manual fingerprint classification was performed by inspecting the geometric characteristics of major ridge curves in a fingerprint image called orientation field flow curves (OFFCs). Lately, a method has been presented for the detection of a fingerprint's reference point by analyzing fingerprint ridges curvatures, see [18], in which the total execution times of the most important stages was 143 ms. In Castillo-Rosado and Hernández-Palancar [19], a new fingerprint feature has been introduced, named Distinctive Ridge Point (DRP), combined with an improved triangle-based representation which also used minutiae. This technique needs to decrease the ridge points dependence with minutiae to get better results. Recently, a model of receiver operating characteristic (ROC) curve has been proposed, which depended on a weighted empirical process to jointly account for the order constraint and within-cluster correlation structure, see [20]. In such way, the statistical testing for performance fingerprint matching data needs more time complexity. In Gupta *et al.* [21] a novel technique has been proposed which considered the minutiae density and the orientation field direction for the reconstruction of the fingerprint, but the suggested method for orientation field reconstruction only considered the local orientation pattern.

A Few studies talked about mathematical modeling of the whorl fingerprint specially using the phase portraits of a system of differential equations. The idea of phase portraits in texture modelling can be

*Corresponding author. Email: nesreen.alsharman@wis.edu.jo

Figure 1 (a) Concentric whorl [4], (b) spiral whorl [5], and (c) composite whorl [6].

seen in [22] where a characterizing oriented patterns was proposed using the qualitative differential equation theory to analyze real texture images, but no fingerprint image seems to have been considered. In the thesis by Ford [23], the complex flows were divided into simpler components which are modeled by linear phase portraits and then combined to obtain a model for the entire flow field, this idea was applied to fingerprints in [24].

Fingerprint can be captured as graphical ridge and valley patterns, so the global representation of the above categories of fingerprint's flow-like patterns as a smooth deformation of the phase portrait of a system of differential equations is considered in this paper. Using differential equations in the formularization of the general dynamical system that describes concentric, spiral, and composite whorl fingerprint requires understanding the behavior of the ridges and interpreting the deltas and cores that appear in these classes, and how the singular points that represent the core to whorl and deltas in the patterns of phase portraits look like in the considered model.

The system of differential equations basically has two types of singular points; first type is nondegenerate singular point (The Jacobian matrix of the system has no zero eigenvalues), the second type is degenerate singular point (The Jacobian matrix has at least one zero eigenvalue). For the core to whorl can be represented as center or spiral singular point in the system of differential equations, but the delta can be interpreted as a singular point with three hyperbolic sectors, and there is no such singular point exist. So the closer singular point for the delta is the cusp with cutting appropriate edge of it. To know more information about the cusp, we present the following theorem, including determining some types of degenerate equilibrium points of the planar system that are found in [25]. Assume that the origin is an isolated critical point of the planar system

$$\begin{aligned} \dot{x} &= P(x, y), \\ \dot{y} &= Q(x, y). \end{aligned} \tag{1}$$

where $P(x, y)$ and $Q(x, y)$ are analytic in some neighborhood of the origin, and consider the case when the matrix $A = Df(0)$ has two zero eigenvalues i.e., $det(A) = 0$, $tr(A) = 0$, but $A \neq 0$, in this case the system (1) can be put in the normal form

$$\begin{aligned} \dot{x} &= y, \\ \dot{y} &= a_k x^k \left[1 + h(x)\right] + b_n x^n y \left[1 + g(x)\right] + y^2 R(x, y). \end{aligned} \tag{2}$$

where $h(x)$, $g(x)$, and $R(x, y)$ are analytic in a neighborhood of the origin, $h(0) = g(0) = 0$, $k \geq 2$, $a_k \neq 0$ and $n \geq 1$, see [25].

Theorem 1.1. *(Theorems 2 and 3, page 151 [25]).*

1. *Let $k = 2m + 1$ with $m \geq 1$ in (2) and let $\lambda = b_n^2 + 4(m + 1)a_k$. Then if $a_k > 0$, the origin is a (topological) saddle. If $a_k < 0$, the origin is*
   - *a focus or a center if $b_n = 0$ and also if $b_n \neq 0$ and $n > m$ or if $n = m$ and $\lambda < 0$,*
   - *a node if $b_n \neq 0$, n is an even number and $n < m$ and also if $b_n \neq 0$, n is an even number, $n = m$ and $\lambda \geq 0$,*
   - *a critical point with an elliptic domain if $b_n \neq 0$, n is an odd number and $n < m$ and also if $b_n \neq 0$, n is an odd number, $n = m$ and $\lambda \geq 0$,*

2. *Let $k = 2m$ with $m \geq 1$ in (2). Then the origin is*
   - *a cusp if $b_n = 0$ and also if $b_n \neq 0$ and $n \geq m$,*
   - *a saddle-node if $b_n \neq 0$ and $n < m$.*

It is clear now from the above theorem that if the Jacobian matrix $Df(x_0)$ has two zero eigenvalues, then the critical point x_0 is either a focus, a center, a node, a (topological) saddle, a saddle-node, a cusp, or a critical point with an elliptic domain.

In Zinoun [26], Zinoun used the Taylor polynomials and the normal forms then applied the Theorem 1.1 to formulate some systems of the classes of the whorl fingerprint such as the concentric whorl and the spiral whorl fingerprint which illustrated in Equations (3) and (4), respectively

$$\begin{aligned} \dot{x} &= y, \\ \dot{y} &= -x\left(x^2-1\right)^2. \end{aligned} \tag{3}$$

and

$$\begin{aligned} \dot{x} &= y, \\ \dot{y} &= (y - x/2)\left(x^2-1\right)^2. \end{aligned} \tag{4}$$

In this research, the spiral whorl fingerprint is developed, a new model for composite whorl with "S" core is suggested and all above categories of the whorl fingerprint are generalized in a dynamical system with a parameter θ as follows

$$\ddot{x} - (\theta\dot{x} - x)\left(x^2-1\right)^2 = 0, \quad \theta \in \mathbb{R}. \tag{5}$$

Equation (5) can be written as a first order system

$$\begin{aligned} \dot{x} &= y, \\ \dot{y} &= -x\left(x^2-1\right)^2 + \theta y\left(x^2-1\right)^2, \quad \theta \in \mathbb{R}. \end{aligned} \tag{6}$$

This paper is organized as follows: In the next section, we study the stability of the equilibria of the system (6). In Section 3 an interesting simulations are shown for the three categories of the whorl fingerprint. A brief results are summarized in Section 5.

2. STEADY STATES AND THEIR STABILITY

To study the stability of the system (6), we find the equilibria first, which are the solutions of the following equations:

$$0 = y, \tag{7}$$

$$0 = -x\left(x^2-1\right)^2 + \theta y\left(x^2-1\right)^2. \tag{8}$$

and are given by $E_0 = (0, 0)$, $E_1(1, 0)$, and $E_2 = (-1, 0)$ which are called equilibrium points or singular points. The Jacobian matrix of (6) takes the form

$$J = \begin{bmatrix} 0 & 1 \\ -(x^2-1)^2 + 4(\theta y - x)(x^2-1)x & \theta(x^2-1)^2 \end{bmatrix}. \tag{9}$$

The Jacobian matrix evaluated at the equilibrium point $E_0 = (0, 0)$ is

$$J\left(E_0\right) = \begin{bmatrix} 0 & 1 \\ -1 & \theta \end{bmatrix}. \tag{10}$$

We summarize the stability of E_0 in the following theorem.

Theorem 2.1. *The equilibrium point $E_0 = (0, 0)$ is stable if $\theta < 0$, unstable if $\theta > 0$, and center if $\theta = 0$.*

Proof. From the Jacobian matrix (10), the eigenvalues of $J(E_0)$ are

$$\lambda_{1,2} = \frac{\theta \pm \sqrt{\theta^2 - 4}}{2}. \tag{11}$$

Notice that the eigenvalues of the equilibrium point $E_0 = (0, 0)$ depend only on the parameter θ. When $\theta < 0$, the real parts of the eigenvalues are negative, so E_0 is stable. Similarly, when $\theta > 0$, the real parts of the eigenvalues are positive, and E_0 is unstable. Finally, when $\theta = 0$, we get $\lambda_{1,2} = \pm i$, and so E_0 is center. □

The equilibrium points $E_1 = (-1, 0)$ and $E_2 = (1, 0)$ have the same Jacobian matrix

$$J\left(E_1\right) = J\left(E_2\right) = \begin{bmatrix} 0 & 1 \\ 0 & 0 \end{bmatrix}. \tag{12}$$

We summarize the stability of $E_1 = (-1, 0)$ and $E_2 = (1, 0)$ in the following theorem

Theorem 2.2. *The equilibrium points $E_1 = (-1, 0)$ and $E_2 = (1, 0)$ are cusps.*

Proof. The eigenvalues in this case are $\lambda_{1,2} = 0$ which means degenerate equilibrium points, i.e., $det(J) = 0$, $tr(J) = 0$, but $J \neq 0$. In this case it is shown in the introduction that the system can be put in the normal form to which functions can be reduced in a neighborhood of the degenerate critical points $E_1 = (-1, 0)$ and $E_2 = (1, 0)$ as the following

$$\begin{aligned} \dot{x} &= y, \\ \dot{y} &= \pm\alpha(x \pm 1)^2 + o\left((x \pm 1)^3\right). \end{aligned} \tag{13}$$

Apply Theorem 1.1, $k = 2$, $b_n = 0$, $h(x) = 0$ and $\alpha > 0$ which gives that both $E_1 = (-1, 0)$ and $E_2 = (1, 0)$ are cusps.□

3. SIMULATIONS AND NUMERICAL RESULTS OF THE WHORL FINGERPRINT

A fingerprint picture has a lot of redundant data as it is collected before beginning the simulation. Therefore, to get a correct and appropriate image, the input fingerprint images need to be preprocessed. It is important to solve problems such as photos of scars, too moist or too dry fingertips. Some preprocessed methods such as image enhancement, normalization, filtering, noise reduction, binarization, and thinning can be used to preprocess the fingerprint image, see [27]. Thinning is a basic method that constructs a skeleton for the input fingerprint image because it is a technique that takes a fingerprint binary image and renders the ridges that exist in the print just one pixel wide without altering the overall pattern and

leaving holes in the ridges to create a kind of image skeleton. This method helps us to find the tangential direction of the ridges at a point (x,y), where $0 \leq \theta(x, y) < \pi$ and omits a the redundant data so that the thinning preprocessing step is used before simulation [28]. Figure 2 shows the binarization whorl fingerprint input image and thinning preprocessing for the fingerprint image.

In this section, we display the phase portrait of the system (6) using particular values of the parameter θ and match them with the images in the above categories of the whorl fingerprint. We get similar shape to the concentric whorl at the value $\theta = 0$, around and closed to $\theta = 0$, we get shapes look like to the spiral whorl and when we increase the value of the parameter θ to be around one, we get phase portrait closed to the composite whorl with "S" core. For more details let us go over these cases using Maple software.

3.1. Concentric Whorl Class

The basic features of the concentric whorl are the existence of the circular or elliptical ridges in the middle which are represented by the center in the phase portrait, the two deltas which are represented by the two cusps in the phase portrait in the right and left sides, and we can draw two connections between the deltas through the ridges which are represented by separatrices between the cusps from above and below half planes in the phase portrait. Let us put $\theta = 0$ in the system (6), we get the following system

$$\begin{aligned} \dot{x} &= y, \\ \dot{y} &= -x\left(x^2 - 1\right)^2. \end{aligned} \tag{14}$$

Figure 3 shows the phase portrait of the system (14) using Maple and the image that represents the concentric whorl. It easy to compare and matching center with circular ridges in the middle , the cusps with the deltas, and the separatrices with the connections in both pictures.

(a) (b)

Figure 2 The input [29] and thinning preprocessing for the fingerprint image.

3.2. Spiral Whorl Class

In this type, we go over two kinds of the spiral whorl:

- UR-LL spiral whorl in which there exist an upper right connection (UR connection) between the spiral core and the right delta and a lower left connection (LL connection) between the spiral core and the left delta, see picture (b) in Figure 4.
- LR-UL spiral whorl in which there exist a lower right connection (LR connection) between the spiral core and the right delta and an upper left connection (UL connection) between the spiral core and the left delta, see picture (b) in Figure 5.

To get the first kind of spiral, substitute $\theta = 0.2$ in the system (6), we get the following system

$$\begin{aligned} \dot{x} &= y, \\ \dot{y} &= -x\left(x^2 - 1\right)^2 + 0.2y\left(x^2 - 1\right)^2. \end{aligned} \tag{15}$$

The phase portrait of the system (15) is shown in Figure 4. We can see the similarity between the phase portrait and the image that represents UR-LL spiral whorl by comparing the focus with the spiral core, the cusps with deltas, the upper right orbit (UR orbit) between the focus and the right cusp with the upper right connection (UR connection), and the lower left orbit (LL orbit) between the focus and the left cusp with the lower left connection (LL connection).

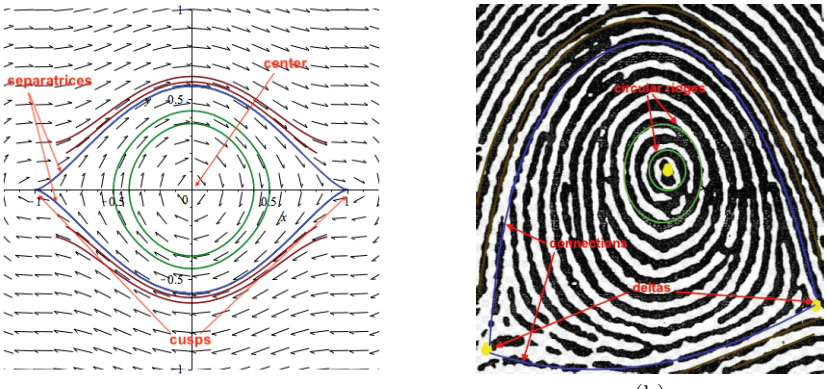

(a) (b)

Figure 3 Simulation of the concentric whorl fingerprint: (a) phase portrait of the system (14) and (b) image [4] of the concentric whorl fingerprint.

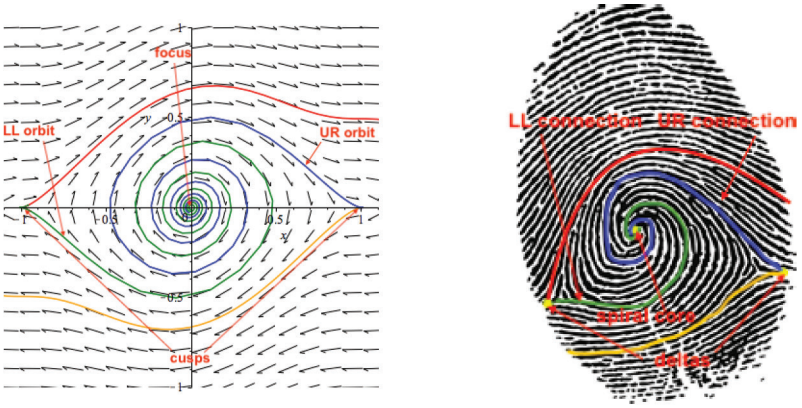

(a) (b)

Figure 4 Simulation of the upper right-lower left (UR-LL) spiral whorl fingerprint: (a) phase portrait of the system (15) and (b) image [5] of the UR-LL spiral whorl fingerprint.

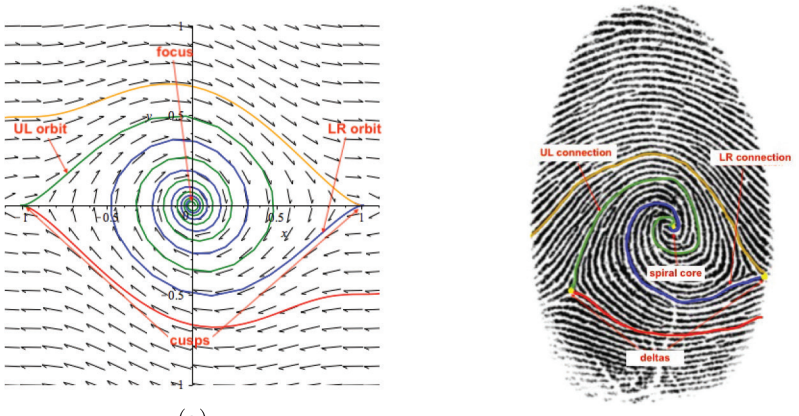

(a) (b)

Figure 5 Simulation of thelower right-upper left (LR-UL) spiral whorl fingerprint: (a) phase portrait of the system (16) and (b) image [5] of the RU-LL spiral whorl fingerprint.

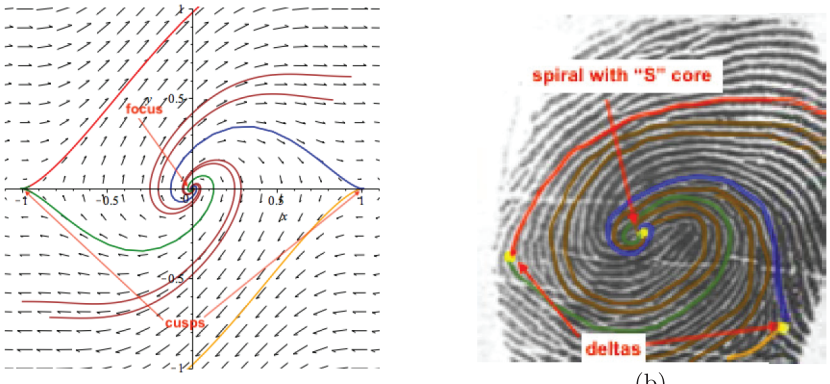

(a) (b)

Figure 6 Simulation of the composite whorl with S core fingerprint: (a) phase portrait of the system (17) and (b) image [6] of the composite whorl with "S" core.

To get the kind LR-UL spiral whorl, we should think how to switch the connections in the Figure 4 up side down, this can be happened if we use negative value of θ, we use $\theta = -0.2$ in the system (6) which is explained in the system (16).

$$\begin{aligned} \dot{x} &= y, \\ \dot{y} &= -x\left(x^2-1\right)^2 - 0.2y\left(x^2-1\right)^2. \end{aligned} \tag{16}$$

Figure 7 | The validation accuracy experiments for retraining VGG16 Convolutional Neural Network (CNN) using MATLAB.

The phase portrait of the system (16) is illustrated in Figure 5 which achieves our target.

3.3. Composite Whorl with "S" Core Class

The composite whorl with "S" core is characterized with a center looks like an "S," and two cusps in the two sides. If θ in the system (6) grows up around one, the flow is twisted enough to create "S" in the middle with keeping the cusps in both sides, consider system (6) with $\theta = 0.9$ we get the following system

$$\begin{aligned} \dot{x} &= y_1, \\ \dot{y} &= -x\left(x^2-1\right)^2 + 0.9y\left(x^2-1\right)^2. \end{aligned} \tag{17}$$

Notice the flow in the phase portrait of the system (17) which is explained in Figures 6 and 7 and the friction ridges of the composite whorl with "S" are almost similar.

4. VGG16 CNN ARCHITECTURE AND RESULTS

After the Maple is used for numerical simulations to the visualizing between orientation field of arch fingerprint's images and phase portraits of the planar proposed dynamical system for preparing the whorl dataset to retained using VGG16 deep learning architecture.

A VGG16 is a Convolutional Neural Network (CNN) architecture that its implementation is running using MATLAB environment with a PC containing 5GB of RAM, 4 Intel cores, i5 (2.0GHz each).

NIST Special Database (SD) 302d [29] is used in this research. SD 302d database is a group of biometric data that collected at the intelligence advanced research project activity's Nail to Nail (N2N) fingerprint challenge. SD 302d specifically consists of auxiliary plain capture devices operated at the N2N fingerprint challenge. The images are distributed in the Portable Network Graphics (PNG) image format. Figure 9 shows arch examples from NIST SD 302d. For more information about NIST SD, see https://www.nist.gov/itl/iad/image-group/nist-special-database-302 [30].

VGG16 uses 3 fully connected layers and 16 convolutional layers. on more than a million images, VGG-16 is trained and can classify images into 1000 object categories . All convolutional layers in VGG16 are 3×3 convolutional layers with 2×2 pooling layers with a stride size of 2 and a stride size of 1 and the same padding [31]. The feature map size is reduced by half after each pooling layer. The last feature map before the fully connected layers is 7×7 with 512 channels and it is expanded into a vector with 25,088 [32]. Figure 8 shows Block diagram of VGG-16 network by three fully connected layers [33].

Figure 7 shows different MaxEpochs experiments after retraining VGG16 using MATLAB. The image data store is divided into 0.7 for training class and 0.3 for validation class using the following fragment MAT LAB code: [imdsTrain, imdsValidation] = splitEachLabel(imds,0.7, "randomized") and the image size is [224 224 3].

The validation accuracy and the elapsed time for the experiments are shown in Table 1. The explanation for increasing elapsed time is that adding more layers to CNNs contributes leads to with more computing time, extracting more features that indicate highly precise results could be achieved. If we compare algorithms that made on a database NIST of fingerprint images specifically on the class whorl, we find that Dass and Jain in [17] have reached to accuracy 93.34%, and Li et al. [11] has reached to accuracy 95.6%. In this research the accuracy is 100%; the main reason for getting this accuracy result is the thinning preprocessing which is the basic method for constructing a skeleton for the input fingerprint image. The skeleton of the input fingerprint image helps the mathematical model in matching and simulation through extracting the basic features of the input image which allow VGG16 deep learning CNNks architecture to classify any image in validation data set in proper class or category.

5. CONCLUSION

The proposed method of this research is an adaptive because it combines between a mathematical model and deep learning feature selection for fingerprint image classification. First, the dynamical system (6) with the parameter θ is a good source to generate different categories of the whorl fingerprint. We have noticed that the shape of the flow of this dynamical system at a particular value of the parameter θ and the shape of the ridges in the corresponding image of a category of the whorl fingerprint are almost identical to each other. The flexibility of the system (6) enable us to simulate a class of whorl depending on how much this class is twisted in either a clockwise or counterclockwise directions. Then the dynamical system is useful for helping artificial intelligence and deep learning tools (such as VGG16 CNN architecture) to categorize database of fingerprint images which allows these tools to be retrained with more accuracy that is shown in Table 2. Future works will be aimed to extend the proposed mathematical model to deal with arch and loop fingerprint images and classify any input fingerprint with deep learning.

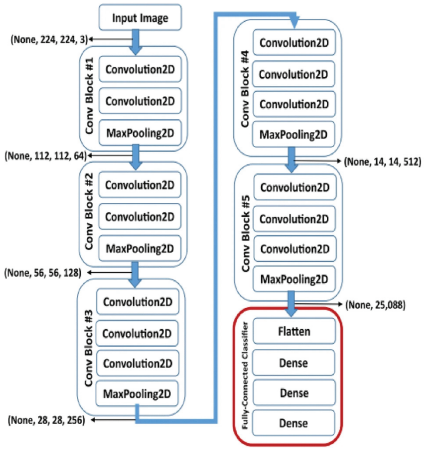

Figure 8 Block diagram of VGG-16 network.

Table 1 The validation accuracy and elapsed time for the experiments.

MaxEpochs	Validation Accuracy (%)	Elapsed Time (sec)
4	40	4
5	60	4
6	80	108
9	80	13
10	100	16

Table 2 Comparison of accuracy in whorl fingerprint classification methods.

Whorl	Accuracy (%)
Dass and Jain method [17]	93.34
Liu Wei method [11]	95.6
Proposed method	100

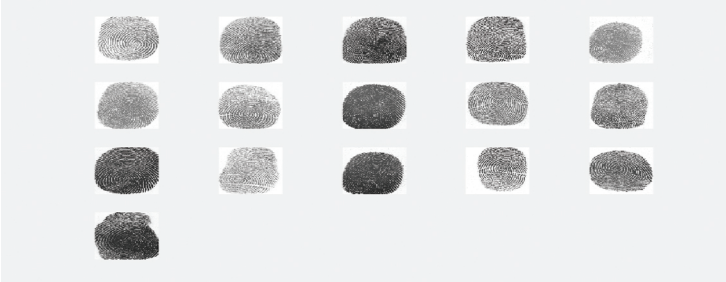

Figure 9 | Whorl examples from NIST special database (SD) 302d [29].

CONFLICTS OF INTEREST

The authors declare no conflicts of interest.

AUTHORS' CONTRIBUTIONS

Authors have contributed to the final version of the manuscript equally.

Funding Statement

This research was funded by all authors.

ACKNOWLEDGMENTS

The authors are indebted to editor and reviewers for their support and for their great comments from which this article has benefited much. They thank their universities AHU and WISE for their assistance.

REFERENCES

[1] F, Galton, Finger Prints, MacMillan and Co., London, England, 1892. https://galton.org/fingerprinter.html
[2] A. de Jongh, A.R. Lubach, S.L. Lie, K.M.A. Ivo Alberink, Measuring the rarity of fingerprint patterns in the dutch population using an extended classification set, J. Forensic Sci. 64 (2019), 108–119.
[3] E.R. Henry, Classification and Uses of Finger Prints, George Rutledge Sons Ltd, London, England, 1990.
[4] Fingerprint analysis. NFSTC, 2013. http://www.forensicsciencesimplified.org/prints/principles.html
[5] Spiralimage. Natalia Connor, 2009. https://www.pinterest.com/nataliaconnor.
[6] Composite whorl. Dermatoglyphics Multiple Intelligence Analysis, Loren Williams, https://slideplayer.com/slide/4877632/16/images/30/Whorl+Family+%3A+Composite+Whorl+%28Wc%29.jpg
[7] G.T. Candela, P. Grother, C. Watson, R.A. Wilkinson, C. Wilson, Pcasys- a Pattern-level Classification Automation System for Fingerprints, NIST, Interagency/Internal Report (NISTIR), US National Institute of Standards and Technology, 29 (1995).
[8] R. Cappelli, A. Lumini, D. Maio, D. Maltoni, Fingerprint classification by directional image partitioning, IEEE Trans. Pattern Anal. Mach. Intell. 21 (1999), 402–421.
[9] A. Jain, S. Prabhakar, L. Hong, A multichannel approach to fingerprint classification, IEEE Trans. Pattern Anal. Mach. Intell. 21 (1999), 348–359.
[10] K. Karu, A.K. Jain, Fingerprint classification, Pattern Recognit. 29 (1996), 389–404.
[11] J. Li, W.-Y. Yau, H. Wang, Combining singular points and orientation image information for fingerprint classification, Pattern Recognit. 41 (2008), 353–366.
[12] H.O. Nyongesa, S. Al-Khayatt, S.M. Mohamed, M.M. Mahmoud, Fast robust fingerprint feature extraction and classification, J. Intell. Robot. Syst. 40 (2004), 103–112.
[13] N.K. Ratha, K. Karu, S. Chen, A.K. Jain, A real-time matching system for large fingerprint databases, IEEE Trans. Pattern Anal. Mach. Intell. 18 (1996), 799–813.
[14] S. Shah, P. Sastry, Fingerprint classification using a feedback-based line detector, IEEE Trans. Syst. Man Cybern. Part B. 34 (2004), 85–94.
[15] Y. Yao, G. Marcialis, M. Pontil, P. Frasconi, F. Roli, Combining flat and structured representations for fingerprint classification with recursive neural networks and support vector machines, Pattern Recognit. 36 (2002), 397–406.
[16] Q. Zhang, H. Yan, Fingerprint classification based on the extraction and analysis of pseudo ridges, Pattern Recognit. 37 (2004), 2233–2243.
[17] S. Dass, A. Jain, Fingerprint classification using orientation field flow curves, in Proceedings of the Fourth Indian Conference on Computer Vision, Graphics & Image Processing, Kolkata, India, 2004, pp. 650–655. https://www.researchgate.net/deref/http%3A%2F%2Fdblp.uni-trier.de%2Fdb%2Fconf%2Ficvgip%2Ficvgip2004.html%23DassJ04
[18] R. Doroz, K. Wrobel, P. Porwik, An accurate fingerprint reference point determination method based on curvature estimation of separated ridges, Int. J. Appl. Math. Comput. Sci. 28 (2018), 209–225.
[19] K. Castillo-Rosado, J. Hernández-Palancar, Latent fingerprint matching using distinctive ridge points, Informatica (Vilnius). 30 (2019), 431–454.
[20] W. Zhang, L.L. Tang, Q. Li, A. Liu, M.-L.T. Lee, Order-restricted inference for clustered ROC data with application to fingerprint matching accuracy, Biometrics. 76 (2020), 863–873.
[21] R. Gupta, M. Khari, D. Gupta, R.G. Crespo, Fingerprint image enhancement and reconstruction using the orientation and phase reconstruction, Inform. Sci. 530 (2020), 201–218.

[22] A.R. Rao, The analysis of oriented textures through phase portraits, in: A Taxonomy for Texture Description and Identification, Springer Series in Perception Engineering, Springer, New York, NY, USA, 1990.
[23] R. Ford, Image models for flow field analysis, representation, and compression: a dynamical systems approach, University Microfilms International, 1994. https://api.semanticscholar.org/CorpusID:60434425
[24] J. Li, W.-Y. Yau, Constrained nonlinear models of fingerprint orientations with prediction, Pattern Recognit. 39 (2006), 39–114.
[25] L. Perko, Differential Equations and Dynamical Systems, vol. 7 of Texts in Applied Mathematics, third ed., Springer-Verlag, New York, NY, USA, 2001.
[26] F. Zinoun, Can a fingerprint be modelled by a differential equation? 2018. https://api.semanticscholar.org/CorpusID:119173983
[27] T. Vidhya, T.K. Thivakaran, Fingerprint image enhancement using wavelet over gabor filters, Int. J. Comput. Technol. Appl. 3 (2012), 1049–1054. http://citeseerx.ist.psu.edu/viewdoc/summary?
[28] I.G. Babatunde, A.O. Charles, A.B. Kayode, O. Olatubosun, Fingerprint image enhancement: segmentation to thinning, Int. J. Adv. Comput. Sci. Appl. 3 (2012). 15–24.
[29] G. Fiumara, P. Flanagan, M. Schwarz, E. Tabassi, C. Boehnen, National Institute of Standards and Technology Special Database 301: Nail to Nail Fingerprint Challenge Dry Run, Technical Note 2002, National Institute of Standards and Technology, 2018.
[30] NIST, NIST special database 302, 2018. https://www.nist.gov/itl/iad/image-group/nist-special-database-302
[31] D. Theckedath, R.R. Sedamkar, Detecting affect states using vgg16, resnet50 and se-resnet50 networks, SN Comput. Sci. 1, 79 (2020).
[32] Q. Guan, Y. Wang, B. Ping, D. Li, J. Du, Y. Qin, H. Lu, X. Wan, J. Xiang, Deep convolutional neural network vgg-16 model for differential diagnosing of papillary thyroid carcinomas in cytological images: a pilot study, J. Cancer. 10 (2019), 4876–4882.
[33] K. Gopalakrishnan, S.K. Khaitan, A. Choudhary, A. Agrawal, Deep convolutional neural networks with transfer learning for computer vision-based data-driven pavement distress detection, Constr. Build. Mater. 157 (2017), 322–330.